

## TECHNICAL REPORT

## Small field of view nuclear imaging detector evaluation using Tc-99m and Ga-67 radioisotopes

M. Georgiou,<sup>a,1</sup> E. Fysikopoulos,<sup>b</sup> M. D'Ignazio,<sup>c</sup> L. Montalto,<sup>c</sup> S. David,<sup>a</sup> L. Scalise<sup>c</sup> and G. Loudos<sup>a</sup>

<sup>a</sup>*Department of Biomedical Engineering, University of West Attica, Athens, Greece*

<sup>b</sup>*BioEmission Technology Solutions R&D, Athens, Greece*

<sup>c</sup>*Dipartimento di Ingegneria, Industriale e Scienze Matematiche, Università Politecnica delle Marche, Ancona, Italy*

E-mail: [georgioumr@gmail.com](mailto:georgioumr@gmail.com)

**ABSTRACT:** In this work we report the imaging performance of a small field of view planar scintigraphic system for low and medium energy radiotracers imaging. <sup>99m</sup>Tc (140 keV) and <sup>67</sup>Ga (93 keV (P1, 42%), 184 keV (P2, 21%), 300 keV (P3, 17%), 393 keV (P4, 5%)) radioisotopes were used to evaluate the nuclear imaging detector in terms of non-uniformity, energy resolution, system spatial resolution and system sensitivity. Moreover, detector's ability to reliably quantify activity variations in the useful field of view has been evaluated. Specific collimator for given photon energy range is needed, in order to reduce image degradation due to photon scattering and penetration. Three parallel hole collimators different in geometry were studied. Results show that all of them are suitable for <sup>99m</sup>Tc and <sup>67</sup>Ga molecular imaging applications, given that only the first photopeak in the case of <sup>67</sup>Ga has to be used for imaging. In this case, accurate quantitative information is obtained with all 3 collimators for both radioisotopes. For <sup>99m</sup>Tc the most appropriate collimator is the one with the thinner septa walls and the lower height, while for <sup>67</sup>Ga the thickest septa and higher height collimator. Dual isotope imaging is applicable using appropriate energy windows and appropriate collimator depending on the application.

**KEYWORDS:** Detector design and construction technologies and materials; Gamma detectors (scintillators, CZT, HPG, HgI etc)

<sup>1</sup>Corresponding author.

---

## Contents

<b>1</b>	<b>Introduction</b>	<b>1</b>
<b>2</b>	<b>Materials and methods</b>	<b>2</b>
2.1	SPECT system	2
2.2	Performance evaluation	3
2.2.1	Flood source correction	3
2.2.2	System uniformity	3
2.2.3	Energy resolution	4
2.2.4	Spatial resolution and sensitivity	4
2.2.5	Activity quantification	4
<b>3</b>	<b>Results</b>	<b>4</b>
3.1	System uniformity	4
3.2	Energy resolution	6
3.3	Spatial resolution and sensitivity	6
3.4	Activity quantification	7
<b>4</b>	<b>Discussion and conclusions</b>	<b>8</b>

---

## 1 Introduction

Single photon emission computed tomography (SPECT) is a tomographic imaging modality that use a radiotracer to assess bodily functions in order to diagnose and/or treat disease diagnose and treat disease. Although SPECT has been used as a clinical tool for several decades, it is also well suited to imaging small animals, like mice, playing an important role in the development of new imaging agents, genetic research and pathophysiologic investigations [1]. In nuclear medicine, following radioactive decay, high energy photons are emitted in all directions exiting the body to be detected by a gamma camera. Therefore, a collimator, which maps lines of response to particular detector positions, is used. Collimators allow only those photons travelling along desired paths to pass through [2]. Specific collimator for given photon energy range is needed, in order to reduce image degradation due to photon scattering and penetration. Moreover, the choice of the collimator has a major impact on the sensitivity and spatial resolution of the imaging system. The principles of collimator design have been extensively described previously [3, 4]. The most commonly used type of collimator in preclinical imaging is the parallel-hole, which consists of a lead/tungsten plate with all of the holes to be parallel to each other. Several types of hexagonal parallel-hole collimators are commercially available differing in geometric characteristics such as septa thickness, holes diameters and holes length. The selection of the appropriate geometric characteristics is crucial as it directly affects the penetration rate in the collimator, for given radioisotope energy. The goal of

this study is the performance evaluation of a small field of view planar scintigraphic system for low and medium energy radiotracers imaging:  $^{99m}\text{Tc}$  (140 keV), which is the most common radioisotope for diagnosis and  $^{67}\text{Ga}$  (photon energies of 93 keV (P1, 42%), 184 keV (P2, 21%), 300 keV (P3, 17%), and 393 keV (P4, 5%)) which is largely used in acute and chronic infection, inflammation, and lymphoma scintigraphy scans [5–7]. Three parallel hole collimators with different geometry have been evaluated in terms of detector non-uniformity, energy resolution, system spatial resolution and system sensitivity. Moreover, detector's ability to reliably quantify activity variations in the useful field of view has been evaluated. In vivo activity quantification is an important task in nuclear medical imaging, as it enables diagnostic or therapeutic decisions based on estimates of activity in objects or regions in the body. All measurements were conducted according to previously published literature relevant to small field of view gamma cameras evaluation [8–12]. The present work constitutes an extended version of a previously-published proceedings paper containing preliminary results of the current evaluation [13].

## 2 Materials and methods

### 2.1 SPECT system

The detection system consists of a pixelated sodium iodide activated with thallium (NaI(Tl)) crystal (SaintGobain, France) with an area of  $97.4 \times 44.8 \text{ mm}^2$ . The discrete pixel dimensions are  $1 \times 1 \times 5 \text{ mm}^3$  with a pitch of 1.2 mm glued through an optical grease BC-630 (SaintGobain, France) to a pair of H8500C flat-panel Position Sensitive Photomultiplier Tubes (PSPMTs — Hamamatsu Photonic Co., Japan) in a  $1 \times 2$  arrangement with total dimensions of  $105.7 \times 52 \times 34 \text{ mm}^3$ . The scintillator array is housing by an aluminum cover 50  $\mu\text{m}$  thick and coupled to photodetectors array through a 3 mm glass window. Three hexagonal parallel hole collimators with different geometry were used:

- lead collimator with holes of 1.2 mm inner diameter, 0.2 mm septa and 25 mm height (Tecomet Inc.);
- tungsten collimator with holes of 1.2 mm inner diameter, 0.3 mm septa and 28 mm height (LayerWise, NV);
- tungsten collimator with holes of 1.2 mm inner diameter, 0.5 mm thick septum walls and 30 mm height (LayerWise, NV).

The theoretical penetration rate, calculated according to an online design calculator [14], is summarized in table 1.

The system is enclosed in an 8 mm thick tungsten (W) housing box with dimensions equal to  $140 \times 82 \times 107 \text{ mm}^3$ . Each of the PSPMT provides 64 output signals which were reduced to 4 position through a Symmetric Charge Division (SCD) Circuit [15]. Four custom pre-amplifiers at the end of the resistive chain shape the position signals, taking into account the analog to digital conversion (ADC) sampling rate. The four positions signals from each PSPMT were digitized at 50 MHz sampling rate using 12-bit resolution free running analog to digital converters (ADC) (Texas Instruments ADS5282). The sampling is continuous, in order to record the whole pulse and get the maximum of information. An embedded system based on MicroBlaze microprocessor (Xilinx Inc, US) was

**Table 1.** Theoretical penetration rate.

Penetration (%)	Tc-99m	Ga-67	Ga-67	Ga-67
Energy photopeak (keV)	140	93	184	300
Collimator 1	0.41	0.03	6.1	48.2
Collimator 2	0.01	0	1.04	28.9
Collimator 3	0	0	0.05	11.9

developed at a Spartan 6 LX150T FPGA development board (Avnet Inc, US) for data acquisition and processing of the digitized signals. The data acquisition system architecture is described in detail in [16]. The optimal high voltage was found to be equal to -865V for technetium-99m ( $^{99m}\text{Tc}$ ) imaging and -920V for gallium-67 ( $^{67}\text{Ga}$ ) imaging, in order to be able to acquire only the two (P1 and P2) of the four photopeaks. P3 and P4 gammas have higher probability of Compton interactions in the object and the collimator and therefore consequent loss of spatial information in the images.

## 2.2 Performance evaluation

Performance parameters including detector non-uniformity, energy resolution, system spatial resolution, system sensitivity and quantification were measured previously published literature [8–12]. An energy window of  $\pm 20\%$  has been applied around the photopeaks in all measurements following the promising results of a similar, recently commercial, dedicated scintigraphic system [11].

### 2.2.1 Flood source correction

Position mapping and uniformity correction is a standard practice for pixelated scintillator based small field of view scintigraphic systems [17, 18]. PSPMTs are a basic component of a gamma ray detector and behave in a non-uniform manner, since each anode show a slightly different response. The correction methods include position mapping, uniformity correction and energy correction. Position mapping was achieved by placing 10  $\mu\text{Ci}$  point sources ( $^{99m}\text{Tc}$  and  $^{67}\text{Ga}$ ) at one meter above the scintillator without collimation. Using the obtained raw flood images, a grid that maps each crystal pixel was determined for both radioisotopes respectively. An energy window of  $\pm 20\%$  around each corresponding photoelectric peak has been applied in each crystal pixel for energy correction. Afterwards, a plastic container filled with radioactive solution (400  $\mu\text{Ci}$  in case of  $^{99m}\text{Tc}$  and 200  $\mu\text{Ci}$  in case of  $^{67}\text{Ga}$ ) was placed upon the detector for each three collimators. Both flat sources were sufficiently large to cover the entire detector and were placed in direct contact with the collimated detector. A large number of counts ( $2 \times 10^6$ - $4 \times 10^6$ ) were collected in each case to minimize the statistical noise. The counts in each crystal pixel have been summed, leading to the flood matrix, which corrects the intensity of the raw images.

### 2.2.2 System uniformity

System uniformity was measured on flood images, produced as described above, for each collimator. The flood images were smoothed processed with a 9-point smoothing filter with the following weightings [1 2 1; 2 4 2; 1 2 1] according to previous published procedures for the evaluation of

detectors non-uniformity [17–20]. Mean value and standard deviation of the pixel counts in the central 75% of the images area were calculated. The ratio between the standard deviation and the mean value was reported as system uniformity.

### 2.2.3 Energy resolution

The intrinsic ability of a detector to distinguish  $\gamma$  rays of different energies is reflected in its energy resolution. 10  $\mu\text{Ci}$   $^{99m}\text{Tc}$  and  $^{67}\text{Ga}$  point sources were used for the irradiation of the detector without collimation. In both occasions the point source was placed at 1 m distance apart from the surface of the scintillator. For each crystal pixel, the energy spectrum was acquired and an automated algorithm was used to find and record the corresponding photopeak channel in all pixels. All spectra were normalized to the same photopeak position by multiplying each value of the spectrum with the ratio of the selected normalized photopeak with the current photopeak. The normalized energy spectrum is the sum of all individual spectra, after applying these corrections for each independent crystal elements of the array. A Gaussian fit was applied to the normalized energy spectrum around each corresponding photopeak and the energy resolution was determined for the corresponding energy peak, using the standard Full Width at Half Maximum (FWHM) [21].

### 2.2.4 Spatial resolution and sensitivity

In order to estimate the system spatial resolution and sensitivity, a capillary tube filled with the corresponding radioisotope (50  $\mu\text{Ci}$ - $^{99m}\text{Tc}$ , 50  $\mu\text{Ci}$ - $^{67}\text{Ga}$ ) was used. The capillary having an inner diameter of 0.6 mm, external diameter of 1.40 mm and 60 mm length was placed with a slight inclination at different distances from the collimator, for all three collimators used in this study. Spatial resolution was calculated as the mean FWHM of the line spread function (LSF) produced by several line profiles along the capillary length, for each distance. Sensitivity (counts/min/ $\mu\text{Ci}$ ) was calculated as the recorded counts per minute in the corrected image divided by the decay-corrected activity of the source.

### 2.2.5 Activity quantification

For the evaluation of system sensitivity to activity variations, 3 cylindrical phantoms (10 mm in diameter) filled with 1 ml of radioisotope solutions were placed directly upon the collimator. A dose calibrator was used in order to measure the preciseness of phantoms activity ratio. The measured activities for  $^{99m}\text{Tc}$  were: 14  $\mu\text{Ci}$  (1), 26  $\mu\text{Ci}$  (2) and 55  $\mu\text{Ci}$  (3) corresponding to actual ratios of approximately 0.54 (1:2) and 0.25 (1:3). In the case of  $^{67}\text{Ga}$  the measured activities were: 12.3  $\mu\text{Ci}$  (1), 23.9  $\mu\text{Ci}$  (2) and 46.3  $\mu\text{Ci}$  (3), corresponding to actual ratios of approximately 0.52 (1:2) and 0.27 (1:3). The aforementioned ratios were also measured on the acquired images and the results were compared in order to determine and quantify deviations.

## 3 Results

### 3.1 System uniformity

The uniformity values are summarized in table 2. Results show that all three collimators can be used for  $^{99m}\text{Tc}$  imaging, finding the first collimator to be the most appropriate. The corresponding

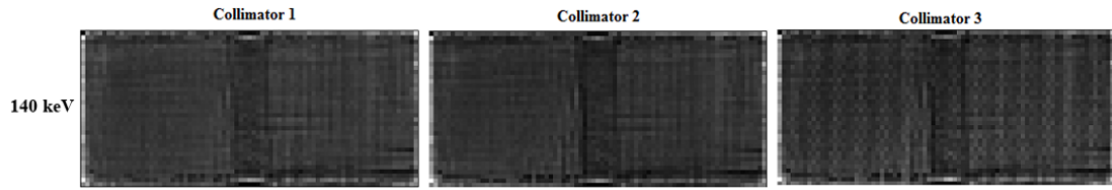


**Figure 1.** Flood images acquired with  $^{99m}\text{Tc}$ .

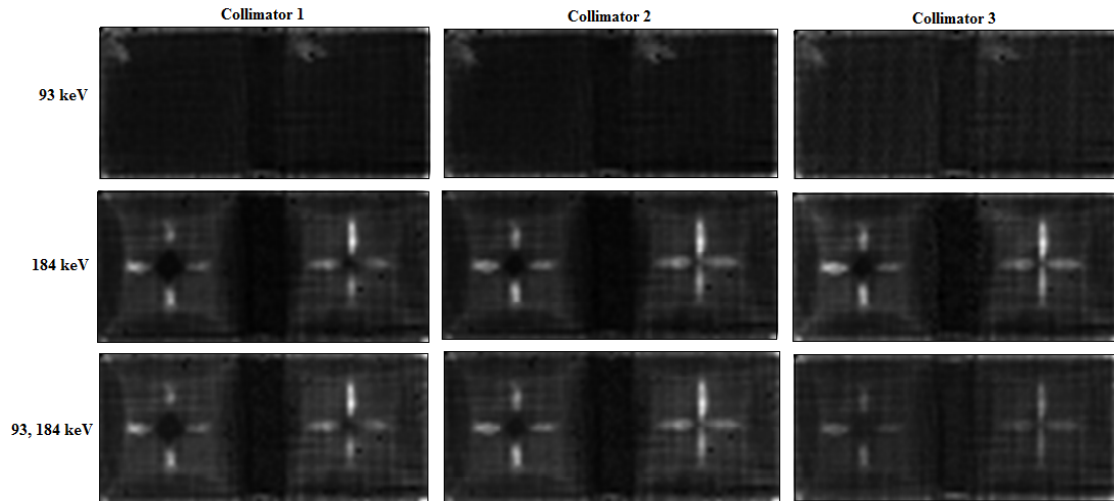


**Figure 2.** Flood images acquired with  $^{67}\text{Ga}$ .

**Table 2.** System uniformity.

System uniformity (%)	Tc-99m	Ga-67	Ga-67	Ga-67
Energy photopeak (keV)	140	93	184	93 & 184
Collimator 1	9.5	40	66	54
Collimator 2	12	39	71	59
Collimator 3	15	28	64	46

acquired flood images are illustrated in figure 1. As far as concern  $^{67}\text{Ga}$ , one can observe that using the second photopeak (P2: 184 keV) for imaging, significantly degrades system's uniformity in all occasions. Higher penetration rates of P3 (300 keV) and P4 (393 keV) gammas, probably leads to its detection inside the energy window applied around the second photopeak (P2: 184 keV). Trying to avoid this degradation one should use only the first photopeak (P1: 93 keV) for imaging, for all three collimators. The calculated uniformity values, using only the first photopeak for imaging, indicate that it is not prohibitive to use all three collimators, finding collimator 3 the most appropriate. The corresponding acquired flood images are illustrated in figure 2.

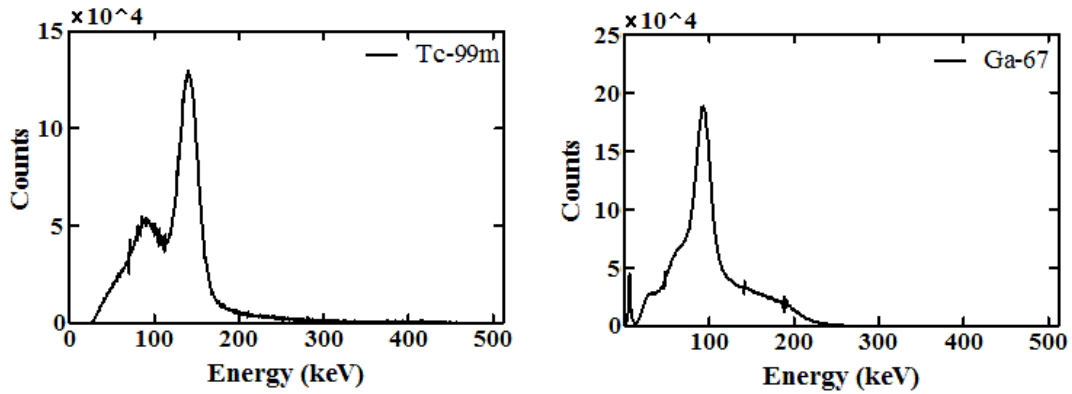


**Figure 3.** Normalized energy spectra for  $^{99m}\text{Tc}$  (left) and  $^{67}\text{Ga}$  (right) irradiation respectively.

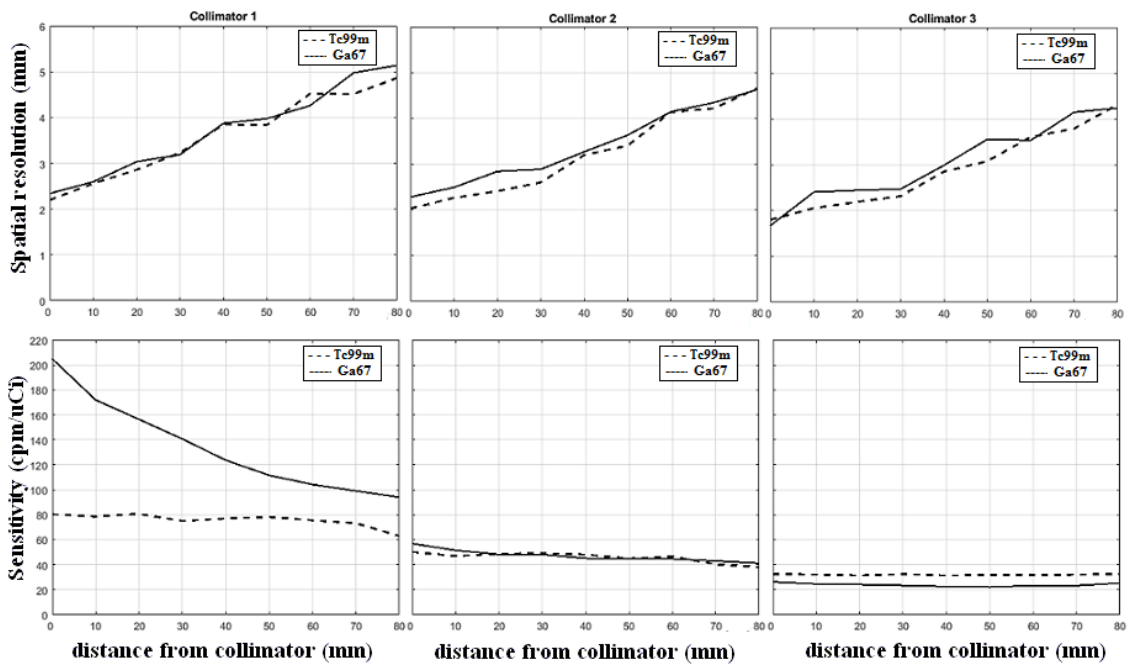


**Figure 4.** Measured system spatial resolution (FWHM) and sensitivity as a function of distance from the detector surface for  $^{99m}\text{Tc}$  and  $^{67}\text{Ga}$  imaging using a  $\pm 20\%$  energy window around 140 keV and 93 keV photopeaks respectively.

### 3.2 Energy resolution

The energy resolution was measured equal to 19.2% for  $^{99m}\text{Tc}$  and 28% for  $^{67}\text{Ga}$ . Figure 3 presents the normalized energy spectra for  $^{99m}\text{Tc}$  and  $^{67}\text{Ga}$  respectively.

### 3.3 Spatial resolution and sensitivity

Figure 4 shows the measured system's spatial resolution (FWHM) and sensitivity as a function of distance from the detector surface for  $^{99m}\text{Tc}$  and  $^{67}\text{Ga}$ . Only the first photopeak of  $^{67}\text{Ga}$  was used for imaging. In case of  $^{99m}\text{Tc}$ , the FWHM is 2.2 mm at zero source to collimator distance and 3.2

**Table 3.** Performance parameters for Tc-99m (140 keV).

	Collimator 1	Collimator 2	Collimator 3
Energy resolution (%)		19.2	
Spatial resolution (at 0mm) (mm)	2	2	1.8
Spatial resolution (at 30mm) (mm)	2.8	2.6	2.3
Sensitivity (at 30mm) (cpm/ $\mu$ Ci)	75	48	32

**Table 4.** Performance parameters for Ga-67 (93 keV).

	Collimator 1	Collimator 2	Collimator 3
Energy resolution (%)		28	
Spatial resolution (at 0mm) (mm)	2.3	2.3	2
Spatial resolution (at 30mm) (mm)	3.2	2.9	2.8
Sensitivity (at 30mm) (cpm/ $\mu$ Ci)	140	48	23

mm at 30 mm far distance for collimator 1; 2 mm at zero source to collimator distance and 2.9 mm at 30 mm far distance for collimator 2; 1.8 mm at zero source to collimator distance and 2.3 mm at 30 mm far distance for collimator 3. System sensitivity is equal to  $\sim 80$  cpm/ $\mu$ Ci for collimator 1;  $\sim 50$  cpm/ $\mu$ Ci for collimator 2; and  $\sim 40$  cpm/ $\mu$ Ci for collimator 3, for all distances examined.

For  $^{67}\text{Ga}$  imaging (P1 only) the FWHM is 2.3 mm at zero distance and 3.2 mm at 30 mm far distance for collimator 1; 2.3 mm at zero distance and 2.9 mm at 30 mm far distance for collimator 2; 1.7 mm at zero distance and 2.5 mm at 30 mm far distance for collimator 3. System sensitivity degrades from  $\sim 200$  cpm/ $\mu$ Ci to  $\sim 100$  cpm/ $\mu$ Ci for collimator 1 as the distance to collimator increases due to the relatively high penetration rate of the 184 keV photons in this collimator (table 1);  $\sim 50$  cpm/ $\mu$ Ci for collimator 2; and  $\sim 30$  cpm/ $\mu$ Ci for collimator 3, for all distances. Performance parameters for all setups are summarized in tables 3 and 4.

### 3.4 Activity quantification

The corrected images with the 3 cylindrical phantoms used for the evaluation of system sensitivity dependency to activity variations for  $^{99m}\text{Tc}$  and  $^{67}\text{Ga}$  are illustrated in figure 5 and figure 6 respectively (from left to right: (3),(2),(1)). In the case of  $^{99m}\text{Tc}$ , the measured activities ratios (1:2 and 1:3) in the corrected image was equal to 0.5 and 0.24 for collimator 1; 0.47 and 0.25 for collimator 2; and 0.48 and 0.22 for collimator 3, reliably quantify the actual activities ratios measured in the dose calibrator (0.54 and 0.25). In the case of  $^{67}\text{Ga}$ , the measured activities ratios in the corrected image, when only the first photopeak was used for imaging, was equal to 0.54 and 0.34 for collimator 1; 0.51 and 0.29 for collimator 2; and 0.46 and 0.26 for collimator 3, reliably quantify the actual activities ratios measured in the dose calibrator (0.52 and 0.27). When using also the second photopeak for imaging the measured ratios were far beyond from the actual ones. Moreover, one can observe the

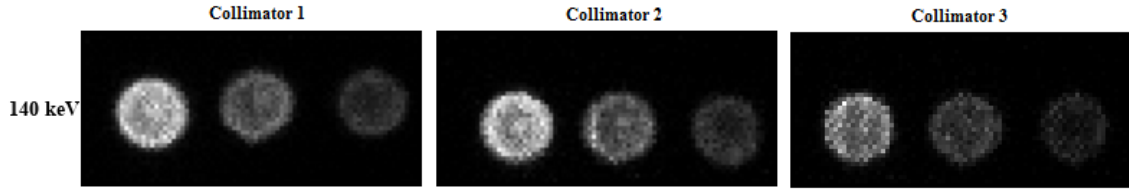


**Figure 5.** Three cylindrical phantoms (10 mm in diameter) filled with  $^{99m}\text{Tc}$  solutions of different activities — from left to right: (3), (2), (1).

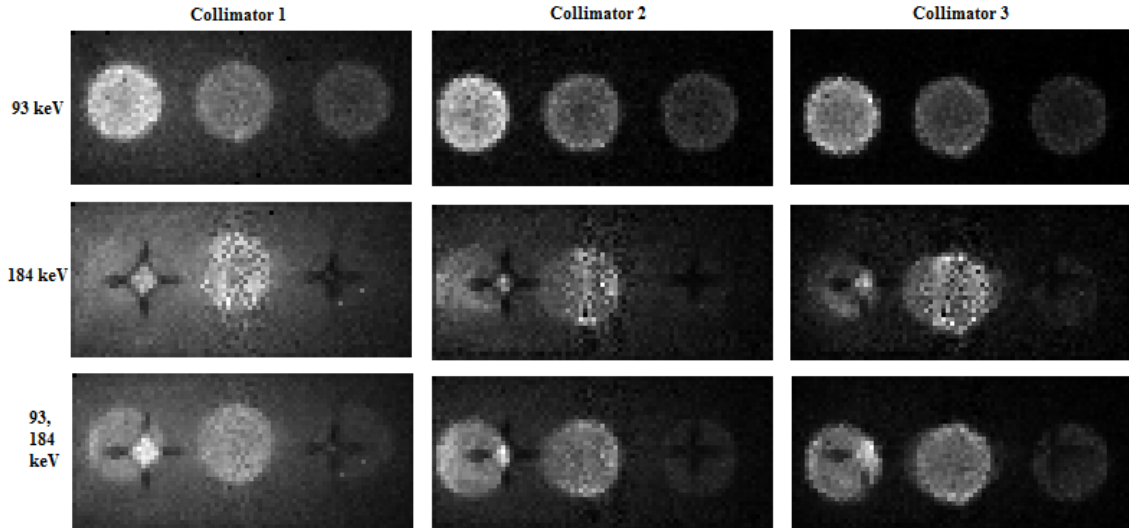


**Figure 6.** Three cylindrical phantoms (10 mm in diameter) filled with  $^{67}\text{Ga}$  solutions of different activities — from left to right: (3), (2), (1).

image quality degradation for all three collimators when the second photopeak of  $^{67}\text{Ga}$  is used for imaging, resulting in loss of the quantitative information (figure 6 —  $2^{\text{nd}}$  and  $3^{\text{rd}}$  row). Finally, the deviation of the measured ratio from the actual one measured with a dose calibrator, in each case, is reported in table 5. To conclude, accurate quantitative information is obtained with all collimators for  $^{99m}\text{Tc}$  imaging and for  $^{67}\text{Ga}$  using only the first photopeak for imaging.

#### 4 Discussion and conclusions

This study presents the performance evaluation of a small field of view scintigraphic planar camera for  $^{99m}\text{Tc}$  and  $^{67}\text{Ga}$  molecular imaging applications. Three parallel hole collimators with different geometry have been evaluated in terms of detector non-uniformity, energy resolution, system spatial resolution, system sensitivity and activity quantification.

As expected, for  $^{99m}\text{Tc}$  imaging the appropriate collimator is the one with the thinnest septa and the lowest height (i.e collimator 1) providing the best spatial resolution to sensitivity compromise and better uniformity, compared to the other two collimators. Accurate quantitative information is obtained with all 3 collimators, proving the ability to reliably quantify activity variations, which is increasingly important in small animal molecular imaging applications, in which it is essential to

**Table 5.** Deviation of measured ratio from actual one.

Radio-isotope	ratio	Deviation(%) Collimator 1	Deviation(%) Collimator 2	Deviation(%) Collimator 3
$^{99m}\text{Tc}$ 140 keV	(1)/(2)	4	7	6
	(1)/(3)	1	0	3
$^{67}\text{Ga}$ 93 keV	(1)/(2)	2	1	6
	(1)/(3)	7	2	1
$^{67}\text{Ga}$ 184 keV	(1)/(2)	18	26	33
	(1)/(3)	17	3	13
$^{67}\text{Ga}$ 93,184 keV	(1)/(2)	14	22	23
	(1)/(3)	12	0	4

quantify the uptake of radioactivity in small organs or tissues which corresponds to the metabolic activity of the injected radiopharmaceutical. The results are directly comparable with a commercially available similar small field of view scintigraphic imaging system [11]. As the septa thickness and the height of collimators holes increases (i.e. collimator 2 and 3), spatial resolution improves, while system uniformity and sensitivity decreases, as expected.

For  $^{67}\text{Ga}$  similar results were obtained for collimator 2 and 3, regarding system spatial resolution and sensitivity, using only the first photopeak (P1: 93 keV) for imaging. Results are similar with those obtained using  $^{99m}\text{Tc}$  and these collimators. As far as concern image uniformity, we conclude that the presence of high energy gamma rays in  $^{67}\text{Ga}$  decay scheme lead to two problems: photon scattering and collimator wall penetration. We strongly believe that the artifacts introduced in the flood images (figure 1) come from P3 (300 keV) and P4 (393 keV) penetrated and scattered events that have been detected in the energy window applied around the second photopeak (P2: 184 keV). On the other hand, photons that are scattered to the collimator without penetration, introduce an overall background leading to relatively poor uniformity observed in all three collimators. This is especially true for the first collimator, which presents a relative high penetration rate also for 184 keV photons, leading to more blurred images, in comparison with those obtained using the other two collimators. This also affects sensitivity curve in which we observed a degradation of 50% in the recorded counts as the distance to collimator increases from 0 mm to 80 mm, which makes sense from a geometrical point of view. However, the calculated uniformity values indicate that it is not prohibitive to use all three collimators given that only the first photopeak (P1: 93 keV) is used for the imaging. As the septa thickness and the height of collimators holes increases image degradation decreases. Moreover, accurate quantitative information is obtained with all 3 collimators when only the first photopeak is used for imaging. This indicates that  $^{67}\text{Ga}$  imaging is applicable in small animal studies, even with a collimator optimized for  $^{99m}\text{Tc}$ , (collimator 1), allowing the usage of a single system for imaging several radioisotopes. On the other hand, using also the second photopeak for imaging, introduce the cross artifact, probably caused from high energy penetrated events, which reduces detector's ability to reliably quantify activity differentiations.

To conclude, all three collimators are suitable for  $^{99m}\text{Tc}$  and  $^{67}\text{Ga}$  molecular imaging applications given that only the first photopeak in the case of  $^{67}\text{Ga}$  shall be used. For  $^{99m}\text{Tc}$  the most appropriate collimator is the one with the thinner septa walls and the lower height, while for  $^{67}\text{Ga}$  the thickest septa and higher height collimator should be used in order to avoid image degradation due to scattering and collimator wall penetration. Dual isotope imaging is applicable using appropriate energy windows and a) the collimator with the thicker septa walls and the higher height (i.e. collimators 2 and 3), at the expense of relative poor sensitivity as far as concern  $^{99m}\text{Tc}$  imaging; b) the collimator with the thinner septa walls and the lower height (i.e. collimator 1), at the expense of relatively poor uniformity and thus images quality.

## Acknowledgments

This research is implemented through IKY scholarships and co-financed by the European Union (European Social Fund — ESF) and Greek national funds through the action entitled “Reinforcement of Postdoctoral Researchers”, in the framework of the Operational Programme “Human Resources Development Program, Education and Lifelong Learning” of the National Strategic Reference Framework (NSRF) 2014–2020.

## References

- [1] V. Moji et al., *Performance evaluation of a newly developed high-resolution, dual-head animal SPECT system based on the NEMA NU1-2007 standard*, *J. Appl. Clin. Med. Phys.* **15** (2014) 267.
- [2] K.V. Audenhaege et al., *Review of SPECT collimator selection, optimization, and fabrication for clinical and preclinical imaging*, *Med. Phys.* **42** (2015) 4796.
- [3] S. Moore, K. Kouris and I. Cullum, *Collimator design for single photon emission tomography*, *Eur. J. Nucl. Med.* **19** (1992) 138.
- [4] S. Kimiaei, S.A. Larsson and H. Jacobsson, *Collimator design for improved spatial resolution in SPECT and planar scintigraphy*, *J. Nucl. Med.* **37** (1996) 1417.
- [5] S.P. Bartold et al., *Procedure guideline for gallium scintigraphy in the evaluation of malignant disease*, *J. Nucl. Med.* **38** (1997) 990.
- [6] K.A. Morton, J. Jarboe and E.M. Burke, *Gallium-67 imaging in lymphoma: tricks of the trade*, *J. Nucl. Med. Tech.* **28** (2000) 221.
- [7] J. McKillop, I. McKay, G. Cuthbert, I. Fogelman, H. Gray and R. Sturrock, *Scintigraphic evaluation of the painful prosthetic joint: a comparison of gallium-67 citrate and indium-111 labelled leucocyte imaging*, *Clin. Rad.* **35** (1984) 239.
- [8] A.V. Stolin et al., *Characterization of imaging gamma detectors for use in small animal SPECT*, *IEEE Nucl. Sci. Symp. Conf. Rec.* (2003) 2085.
- [9] S. Sajedi et al., *Design and development of a high resolution animal SPECT scanner dedicated for rat and mouse imaging*, *Nucl. Instrum. Meth. A* **741** (2014) 169.
- [10] B.S. Bhatia, S.L. Bugby, J.E. Lees and A.C. Perkins, *A scheme for assessing the performance characteristics of small field-of-view gamma cameras*, *Phys. Med.* **31** (2015) 98.

- [11] M. Georgiou, E. Fysikopoulos, K. Mikropoulos, E. Fragogeorgi and G. Loudos, *Characterization of “ $\gamma$ -eye”: a low-cost benchtop mouse-sized gamma camera for dynamic and static imaging studies*, *Mol. Imag. Biol.* **19** (2016) 398.
- [12] S.L. Bugby, J.E. Lees, B.S. Bhatia and A.C. Perkins, *Characterisation of a high resolution small field of view portable gamma camera*, *Phys. Med.* **30** (2014) 331.
- [13] L. Scalise et al., *Performance evaluation of a small field of view scintigraphic camera for Tc-99m and Ga-67 molecular imaging applications*, in 2018 *IEEE International Symposium on Medical Measurements and Applications (MeMeA)*, *IEEE*, (2018).
- [14] *Collimators for nuclear medicine webpage*, <http://www.nuclearfields.com/collimators-design-calculator.htm>.
- [15] D. Stratos, G. Maria, F. Eleftherios and L. George, *Comparison of three resistor network division circuits for the readout of  $4 \times 4$  pixel SiPM arrays*, *Nucl. Instrum. Meth. A* **702** (2013) 121.
- [16] E. Fysikopoulos, G. Loudos, M. Georgiou, S. David and G. Matsopoulos, *A Spartan 6 FPGA-based data acquisition system for dedicated imagers in nuclear medicine*, *Measur. Sci. Technol.* **23** (2012) 125403.
- [17] Q. Zhang, Y. Lu, K. Yang and Q. Ren, *Position mapping and a uniformity correction method for small-animal SPECT based on connected regional recognition*, *Nucl. Instrum. Meth. A* **704** (2013) 1.
- [18] M.H. Jeong et al., *Performance improvement of small gamma camera using NaI(Tl) plate and position sensitive photo-multiplier tubes*, *Phys. Med. Biol.* **49** (2004) 4961.
- [19] International Atomic Energy Agency, *Quality assurance for SPECT systems*, in *IAEA Human Health Series 6*, IAEA, Vienna, Austria (2009).
- [20] S.R. Cherry, J.A. Sorenson and M.E. Phelps, *Physics in nuclear medicine*, Elsevier/Saunders, Philadelphia, PA, U.S.A. (2012).
- [21] M. Rouchota et al., *A prototype PET/SPECT/X-rays scanner dedicated for whole body small animal studies*, *Hell. J. Nucl. Med.* **20** (2017) 146.